

Article

A Wide-Area Fuzzy Control Design with Latency Compensation to Mitigate Sub-Synchronous Resonance in DFIG-Based Wind Farms

Yaser Bostani ^{1,2,*}, Saeid Jalilzadeh ¹, Saleh Mobayen ^{1,3,*} , Afef Fekih ⁴  and Wudhichai Assawinchaichote ^{5,*} ¹ Department of Electrical Engineering, University of Zanjan, Zanjan 45371-38791, Iran; jalilzadeh@znu.ac.ir² Design and Development Part, Guilan Regional Electric Company, Rasht 41377-18775, Iran³ Future Technology Research Center, National Yunlin University of Science and Technology, Douliou, Yunlin 64002, Taiwan⁴ Department of Electrical and Computer Engineering, University of Louisiana at Lafayette, Lafayette, LA 70504-3890, USA; afef.fekih@louisiana.edu⁵ Department of Electronic and Telecommunication Engineering, Faculty of Engineering, King Mongkut's University of Technology Thonburi, Bangkok 10140, Thailand

* Correspondence: yaser.bostani@gmail.com (Y.B.); mobayen@znu.ac.ir (S.M.); wudhichai.asa@kmutt.ac.th (W.A.)

Abstract: This paper proposes an auxiliary damping control approach based on the wide-area measurement system (WAMS). Its main objective is to mitigate sub-synchronous resonance (SSR) in doubly fed induction generator (DFIG)-based wind farms connected to a series capacitive compensated transmission network. To mitigate the delay in sending measurement signals, typically associated with wide-area measurement systems, a fuzzy logic wide-area damping controller (FLWADC) is considered to mitigate the time delay caused by the phasor measurement unit (PMU) measurement. The FLWADC is a supplementary signal at the stator voltage of the grid-side converter (GSC) of the DFIG-based wind farms. The FLWADC was executed by using the voltage and capacitor voltage variations of the series capacitive compensated transmission network. The effectiveness and validity of the proposed auxiliary damping control was verified using a modified scheme of the IEEE first benchmark model via time-area simulation analysis using MATLAB/Simulink.

Keywords: DFIG; fuzzy controller; measurement systems; latency compensation; sub-synchronous resonance



Citation: Bostani, Y.; Jalilzadeh, S.; Mobayen, S.; Fekih, A.; Assawinchaichote, W. A Wide-Area Fuzzy Control Design with Latency Compensation to Mitigate Sub-Synchronous Resonance in DFIG-Based Wind Farms. *Energies* **2022**, *15*, 1402. <https://doi.org/10.3390/en15041402>

Academic Editor:

Charalampos Baniotopoulos

Received: 7 January 2022

Accepted: 11 February 2022

Published: 15 February 2022

Publisher's Note: MDPI stays neutral with regard to jurisdictional claims in published maps and institutional affiliations.



Copyright: © 2022 by the authors. Licensee MDPI, Basel, Switzerland. This article is an open access article distributed under the terms and conditions of the Creative Commons Attribution (CC BY) license (<https://creativecommons.org/licenses/by/4.0/>).

1. Introduction

Increased power demand, along with the worldwide push for clean energy production, has led to increasing interest in electric power generation using renewable energy sources, especially wind power. DFIG-based, variable-speed wind turbines are the most installed wind generation systems in wind farms. The increased integration of wind farms into the power grid has led to an increased requirement to transmit the generated power to the grid via transmission networks without congestion [1]. Additionally, the need to lower the cost of power production has led to the requirement to increase the power transfer capability of existing transmission lines at the lowest possible cost [2]. Series capacitive compensation of wind farms has emerged as the cost-effective approach to increase the power transfer capability of the transmission lines connecting wind farms to the grid [3]. Though series compensation is a cost-efficient way to decrease the line reactance and improve the system stability and increase the transfer capacity for long transmission lines, series capacitors cause fluctuations with frequencies less than the nominal frequency of the network, known as sub-synchronous resonance (SSR) [4]. Additionally, the increased penetration of DFIG-based wind farms has led to the installation of new substations along series-compensated lines. However, the installation of new substations along existing series-compensated

transmission lines can lead to overcompensated lines (lines with effective series reactance that become capacitive) and further aggravate the SSR problem [5].

The SSR phenomenon is divided into the induction generator effect (IGE) and torsional interaction (TI) in wind farms interfaced with series-compensated transmission lines. In reality, the SSR phenomenon in induction machines is the IGE due to wind generators; the frequency torsional modes can be as little as 1–3 Hz. On the other hand, torsional interaction mode must have a frequency of 57–59 Hz [6]. So far, a large number of studies have been conducted in the field of SSR. Some focused on damping SSR oscillations using an additional controller in the rotor-side converter (RSC) and grid-side converter (GSC) of the DFIG-based wind farm, whereas others emphasized using FACTS devices. For instance, the rotor velocity was used in SSR mitigation control in [7]. Varma et al. explored TCSC and SVC's capability in SSR mitigation in [8]. In [9] investigated SSR in series-compensated, fixed-speed wind generation systems with self-excited, double-cage induction generators. That study showed that the output power from wind farms is inversely proportional to the power system damping. However, most existing wind farms employ DFIG-based, variable-speed wind turbines due to their advantages and ease of control. The study reported in [10] did consider DFIG-based wind turbines; however, only time-domain simulations were considered. No small-signal (eigenvalue) analysis was carried out to understand the damping of modal oscillations related to SSR. The modeling and stability analysis of a DFIG-based wind farm interfaced with series compensation was reported in [11]. The impact of parameters, such as wind speed, compensation level, and current controller parameters, on system damping under sub-synchronous frequency were studied in [12]. However, the study did not differentiate between the two SSR phenomena and overlooked the relationship between the turbine parameters and torsional oscillation modes.

In [13], the IEEE first benchmark model was adopted for the study, and the superiority of the FOPI-based UPFC controller over the PI-based UPFC controller was discussed by comparing the results with various performance indices. A fractional-order PI controller was proposed in [14] to mitigate the sub-synchronous oscillations in the turbine-generator shaft resulting from the sub-synchronous resonance (SSR) stemming from the FACTS devices. In [15], a robust fractional-order PI (FOPI) controller was proposed to decrease the sub-synchronous resonance (SSR) using a static synchronous series compensator (SSSC). The proposed controller was shown to reduce the sub-synchronous oscillations to 4%. In [16], a new approach was proposed for mitigating the problems associated with distance protection by using the synchrophasor measurement. The entire simulation study was investigated using a 48-pulse SSSC and carried out with the Bergeron model of transmission line in PSCAD. However, Wide Area Monitoring Systems (WAMS) are predominantly used in modern power systems; since most wind farms are installed in remote locations far from the compensated power system and transmission lines [17], which is important since the additional controller is for SSR attenuation in DFIG controllers, and this study used voltage and compensator capacitor voltage variations for additional controller inputs. In fact, the measurement of input quantities in WAMS was performed by using phasor measurements units (PMU), which are some of the main components of WAMS. However, the delay of measurement signals by the PMU should be considered in designing the controller as ignoring latency may lead to power system instability [18].

This paper proposes a novel approach for mitigating sub-synchronous resonance (SSR) in DFIG-based wind farms installed in a microgrid with wide area monitoring system (WAMS). Its main contributions are as follows:

- A WAMS-based Fuzzy controller design that takes into consideration communication time latencies resulting from PMU measurement signals.
- A design that reduces sub-synchronous resonance for DFIG-based wind farms.
- Performance analysis is carried out using both time-domain simulations and small signal analysis (eigenvalues).

The remainder of this paper is organized as follows. Section 2 briefly describes the model of the wind power plant under consideration. Section 3 briefly describes the SSR

phenomenon in fixed series compensated DFIG. Section 4 describes the proposed wide-area fuzzy logic controller (FLWADC). Section 5 discusses the simulation results for the case study. Finally, some concluding remarks are given in Section 6.

2. Dynamic Model of the System

Wind farms are typically modeled using the aggregation of several identical wind turbines.

A single line diagram of a DFIG-based wind turbine is depicted in Figure 1. [12,14–17]. Here, X_r represents the transformer reactance, R_L represents the transmission line resistance, X_L the transmission line reactance, X_C the fixed series capacitor, X_S the system’s impedance, whose data are given in the Appendix A (Table A1).

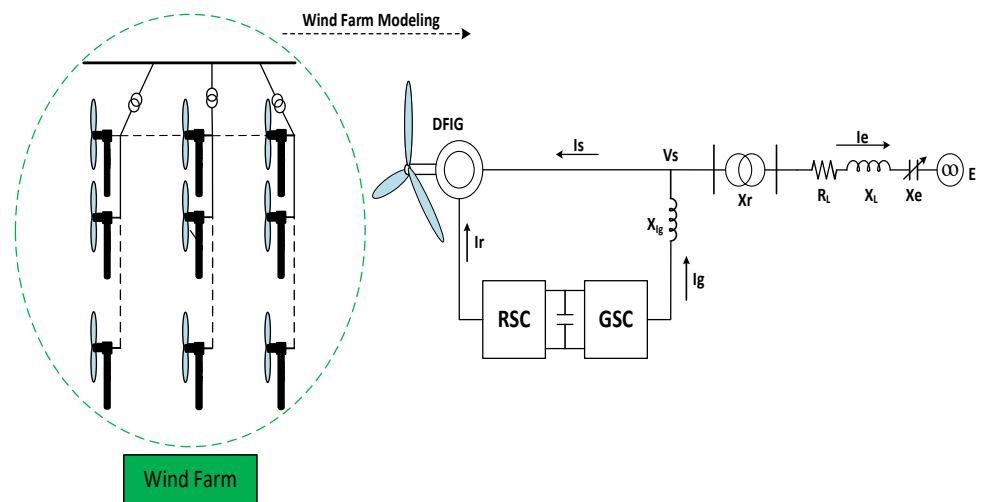


Figure 1. Single Line diagram of a DFIG-based WT.

The dynamic model of each component depicted in the above single line diagram are briefly described below:

2.1. DFIG Model

The DFIG system includes an induction machine and a rotor-side converter (RSC) and a grid-side converter (GSC) connected back-to-back through a dc-link capacitor [18,19]. Assuming negligible magnetic saturation and $X = [i_{qs} \cdot i_{ds} \cdot i_{qr} \cdot i_{dr}]^T$ as the state vector and $U = [V_{qs} \cdot V_{ds} \cdot V_{qr} \cdot V_{dr}]^T$ as control input, the model of an induction machine synchronously rotating in a (dq0) reference frame can be represented as follows [20]:

$$\dot{X} = AX + BU \tag{1}$$

where:

$$A = -\omega_b G^{-1}F$$

$$B = \omega_b G^{-1}$$

$$G = \begin{bmatrix} X_{ss} & 0 & 0 & X_M & 0 & 0 \\ 0 & X_{ss} & 0 & 0 & X_M & 0 \\ 0 & 0 & X_{js} & 0 & 0 & 0 \\ X_M & 0 & 0 & X_{rr} & 0 & 0 \\ 0 & X_M & 0 & 0 & X_{rr} & 0 \\ 0 & 0 & 0 & 0 & 0 & X_{lr} \end{bmatrix} \tag{2}$$

$$F = \begin{bmatrix} R_s & \frac{\omega}{\omega_b} X_{ss} & 0 & 0 & \frac{\omega}{\omega_b} X_M \\ -\frac{\omega}{\omega_b} X_M & R_s & 0 & -\frac{\omega}{\omega_b} X_M & 0 \\ 0 & 0 & R_s & 0 & 0 \\ 0 & \frac{(\omega-\omega_r)}{\omega_b} X_M & 0 & R_r & \frac{(\omega-\omega_r)}{\omega_b} X_{rr} \\ -\frac{(\omega-\omega_r)}{\omega_b} X_{rr} & 0 & 0 & -\frac{(\omega-\omega_r)}{\omega_b} X_M & R_r \end{bmatrix} \quad (3)$$

where ω_b is the base frequency. This latter is equal to the synchronous frequency and is considered to be equal to 314 rad/s per second. ω is the angular frequency of the rotating frame dq. R_s is the stator resistance, R_r the rotor resistance, X_M the magnetic reactance, X_{ls} the stator leakage reactance, and X_{lr} the rotor leakage reactance. $X_{ss} = X_{ls} + X_M$, and $X_{rr} = X_{lr} + X_M$ where the subscripts r and s stand for rotor and stator, respectively. The subscripts d and q stand for direct and quadrature component, respectively.

The RSC and GSC converters, along with their respective proportional integral (PI) controllers, are depicted in Figure 2.

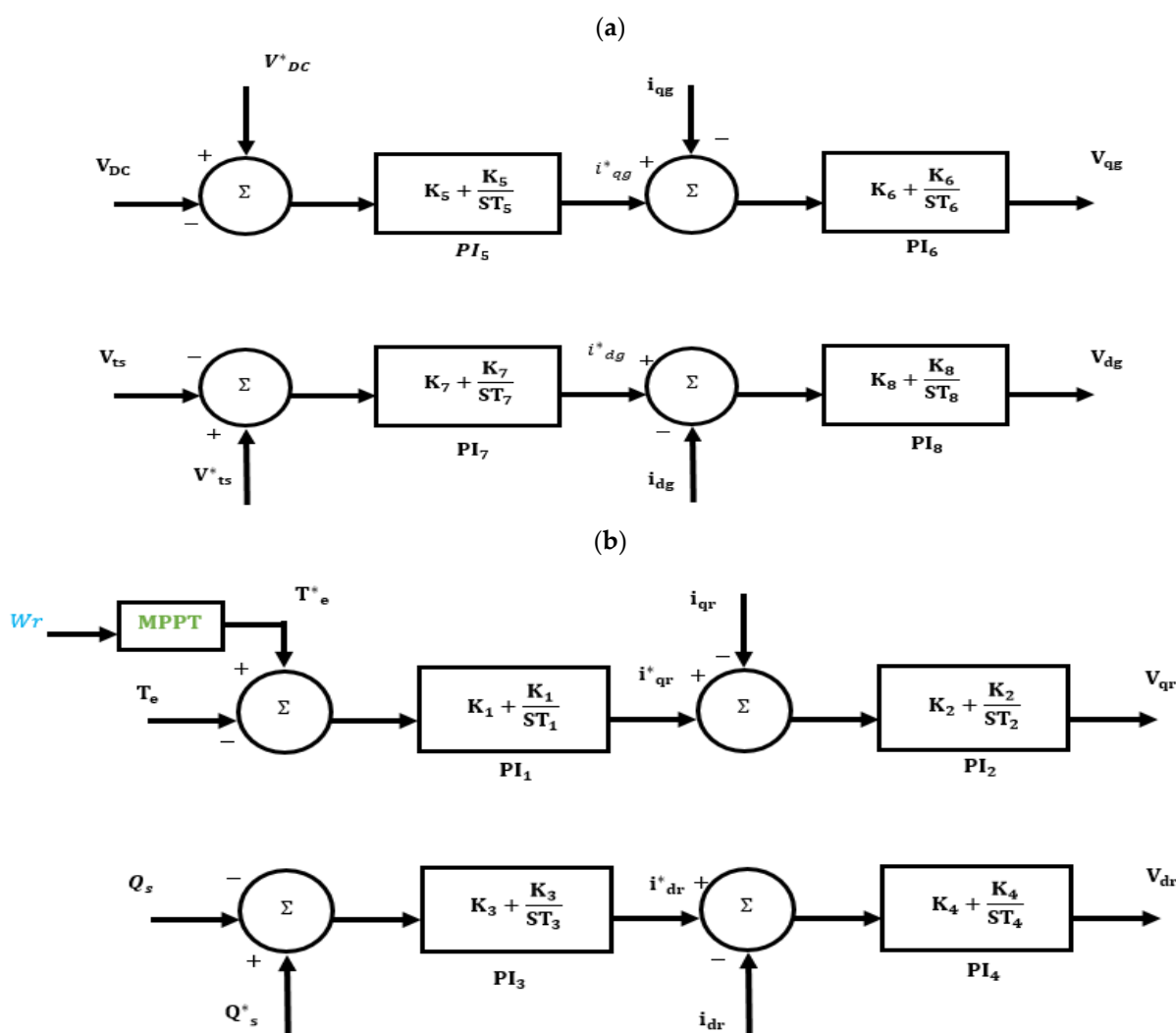


Figure 2. Controllers of the GSC (a) and RSC (b).

Note that the RSC control loops regulate the electromagnetic torque (d-axis loop) and the generator reactive power (q-axis loop), whereas the GSC control loops regulate the DC-link voltage (q-loop) and terminal voltage (d-loop) by providing necessary reactive power [21].

A look-up table-based on Maximum Power Point Tracking (MPPT) is considered to generate the necessary reference torque to ensure maximum power extraction from the wind, as depicted in Table 1.

Table 1. MPPT look-up table.

$V_w(m/s)$	7	8	9	10	11	12
$\omega_r(pu)$	0.75	0.85	0.95	1.05	1.15	1.25
$P_{wind}(pu)$	0.32	0.49	0.69	0.95	1.25	1.6
$T_{wind} = P_{wind}/\omega_r$	0.43	0.58	0.73	0.90	1.09	1.28

The DC-link capacitor connecting the GSC and RSC (Figure 3) can be modeled using the following first order differential equations:

$$cV_{DC} \frac{dV_{DC}}{dt} = -(P_r + P_g) \tag{4}$$

$$P_r = 0.5(V_{qr}i_{qr} + V_{dr}i_{dr}) \tag{5}$$

$$P_g = 0.5(V_{qg}i_{qg} + V_{dg}i_{dg}) \tag{6}$$

where P_r is the true power of the RSC converter, and P_g is the active power of the GSC. V_r , and V_g are the output voltages of the two converters RSC and GSC, respectively [22].

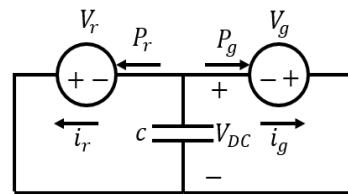


Figure 3. DC-link capacitor of DFIG.

2.2. Model of the Wind Turbine’s Shaft

The wind turbine’s shaft is modeled as follows [23]:

$$\frac{d\omega_t}{dt} = \frac{(-D_t - D_{tg})}{2H_t} \omega_t + \frac{D_{tg}}{2H_t} \omega_r - \frac{1}{2H_g} T_{tg} + \frac{T_{wind}}{2H_t} \tag{7}$$

$$\frac{d\omega_r}{dt} = \frac{D_{tg}}{2H_g} \omega_t + \frac{(-D_t - D_{tg})}{2H_t} \omega_r + \frac{1}{2H_g} T_{tg} + \frac{T_e}{2H_g} \tag{8}$$

$$\frac{dT_{tg}}{dt} = (K_{tg} \cdot \omega_b) \omega_t + (-K_{tg} \cdot \omega_b) \omega_r \tag{9}$$

where ω_t represents the wind turbine’s speed, ω_r depicts the speed of the generator rotor, and T_{tg} is the torsional torque. T_{wind} is the torque generated by the wind, and T_e is the electric torque of the generator.

2.3. Model of the Capacitive Series-Compensated Power Line

The transmission line, along with its capacitors, is modeled as follows [24]:

$$\frac{dI_{qL}}{dt} = \frac{-R_L}{X_L} \omega_b I_{qL} - \omega I_{dL} - \frac{1}{X_L} \omega_b V_{qc} + \left(\frac{1}{X_L} \omega_b \right) (V_{qs} - E_{qB}) \tag{10}$$

$$\frac{dI_{dL}}{dt} = \omega I_{qL} - \frac{R_L}{X_L} \omega_b I_{dL} - \frac{1}{X_L} \omega_b V_{dc} + \left(\frac{1}{X_L} \omega_b \right) (V_{ds} - E_{dB}) \tag{11}$$

$$\frac{dV_{qc}}{dt} = \omega_b X_c I_{qL} - \omega V_{dc} \tag{12}$$

$$\frac{dV_{dc}}{dt} = \omega_b X_c I_{dL} - \omega V_{qc} \quad (13)$$

where V_{qc} and V_{dc} are the series capacitor voltages and currents in the qd0 frame, respectively. V_{qs} , V_{ds} , E_{qB} , and E_{dB} are the stator and the infinite bus voltages in the qd0 reference frame, respectively.

3. SSR and its Methods for Analysis

3.1. Definition of SSR

The SSR phenomenon is the state in which the wind exchanges in one or more natural frequencies energy with the electrical grid. If not prevented, this phenomenon causes damages. The SSR phenomenon is due to two inductive generating effects and the torsional interference effect. In a network with capacitive series compensation, the network has a natural frequency that is calculated by Equation (14); in this relation, the resonant frequency f_n is called sub-synchronous frequency. f_s is synchronous frequency, and X_l is the total reactance of the inductor, transformers, and inductor in Figure 1. X_c is the reactance of a series capacitor, which is a percentage of the reactance. $\frac{X_c}{X_l}$ is called the compensation percentage. Due to frequency f_n , slip S_n is introduced according to Equation (15) [14,19].

$$f_n = f_s \sqrt{\frac{X_c}{X_l}} \quad (14)$$

$$S_n = \frac{f_n - f_r}{f_n} \quad (15)$$

Since S_n is negative, the equivalent resistance of the rotor at the sub-synchronous frequency ($\frac{R_{eq}}{S_n}$) is negative. In other words, f_r is negative when the amplitude of this resistor is more than the sum of the network and armature resistors.

As shown in the second part of Equation (16), the current of the whole system has an exponential function with a positive power. A sub-synchronous component with a frequency of f_n appears in the currents and voltages of the stator and mains circuit with the existence of a capacitive series compensator. The complementary frequency of this component appears as IGE in the rotor current [18].

The torsional mode is the frequency between the two masses of the rotor shaft with a complementary frequency of the network ($f_n - f_r$) equal to or close to it. The torsional interaction (TI) effect occurs when the frequency of the torsional mode between the two masses of the rotor shaft with a complementary frequency of the network ($f_n - f_r$) is equal or close to each other. The frequency of the torsional modes of their rotors is low due to the low stiffness of the rotor shafts of wind farms. Thus, SSR occurs in wind power due to the effect of torsional interaction (TI). Thus, there is a need for a very high level of compensation [25]. In addition, the probability of its occurrence is very low since it requires very high compensation [25].

$$i(t) = A \sin(2\pi f_s t) + e^{\frac{R_{eq}}{L} t} B \sin(2\pi f_n t + \vartheta) \quad (16)$$

3.2. Small-Signal Analysis (System Eigenvalues)

The general state space of the network was modeled around its equilibrium point, depending on wind speed and level of compensation of the capacitor of series, using the linmod command obtained in MATLAB software. In this regard, 20 eigenvalues were obtained from the general state space of the network [26], which were four eigenvalues for the induction machine, three for the shaft system, eight for the RSC and GSR of the DFIG, four for the transmission line with series capacitor, and one for the DC-link which formed the 20th degree model.

Table 2 indicates the system eigenvalues for a compensation level of 70% and wind speed of 8 m/s.

Table 2. Eigenvalues for compensation level 75% at wind speed 7 m/s.

Mode	Eigenvalues	Mode	Eigenvalues
λ_1	+0.273 + j123.26	λ_{11}	−0.023 + j30.56
λ_2	+0.273 − j123.26	λ_{12}	−0.023 − j30.56
λ_3	−6.152 + j628.42	λ_{13}	−109.60
λ_4	−6.152 − j628.42	λ_{14}	−568.235
λ_5	−9.412 + j95.78	λ_{15}	−89.65
λ_6	−9.412 − j95.78	λ_{16}	−0.45
λ_7	−1.150 + j4.260	λ_{17}	−0.254
λ_8	−1.150 − j4.260	λ_{18}	−22.02
λ_9	−189.210 − j1245.45	λ_{19}	−14.25
λ_{10}	−189.210 + j1245.45	λ_{20}	−0.003

Note that all modes are stable except for λ_1 and λ_2 , which represent the unstable sub-synchronous modes for this system.

3.3. Review of Fuzzy System

Fuzzy logic is considered as a method for reasoning which is similar to the way human's reason. The fuzzy logic approach mimics the human decision-making method in which all possible intermediate states between the digital values of "yes" and "no" are considered. Fuzzy logic has four main parts, as discussed below [27].

Rule base: This section includes all of the rules and conditions which are specified as "if then" by an expert and are able to control the decisions of a "decision-making system". Based on the new methods in fuzzy theory, it is possible to adjust and reduce the rules and regulations so that the best results can be obtained with the fewest rules.

Fuzzification: In the fuzzy step, the inputs are converted to fuzzy information. In other words, the numbers and information to be processed become fuzzy sets and numbers. Input data are measured, for example, by sensors in a control system, which are modified and prepared for fuzzy logic processing.

Inference engine: In this section, the degree of compliance of the fuzzy input with the basic rules is determined. In this way, different decisions are generated as a result of the fuzzy inference engine based on the percentage of compliance.

Defuzzification: In the last step, the results of fuzzy inference, which are fuzzy sets, are converted into quantitative data. At this stage, you choose the best decision according to the outputs, which include different decisions with different percentages of compliance. This choice is normally based on the maximum degree of compliance.

4. Proposed Wide-Area Fuzzy Logic Controller (WAFLC)

By combining the capabilities of telecommunication systems and digital measuring devices and controllers, wide-area measurement systems (WAMSs) enable the monitoring, protection, and control of the increasingly complex large power systems. In general, WAMSs consist of three sub-systems, including measurement, telecommunication, and control. The system consists of several phasor measurement units (PMUs) and one or more power distribution systems (PDCs) connected by a high-speed telecommunications network, as shown in Figure 4 [28].

In this study, a WAMS was used to design a fuzzy controller. For this purpose, the PMU, which is one of the main components of WAMSs, was used to measure the compensating voltage of the transmission line series and its changes and was applied to the input of the fuzzy controller. One of the most important items in controller design is choosing the right input signal for the controller, as shown in Figure 2. In this paper, rotor speed (ω_r) and voltage across the series compensation (V_c) were examined, and the optimum input control signal was identified with residue-based analysis, explained in the time-domain simulation results section. Mamdani was used as the fuzzy inference motor. The damping of SSR was achieved by applying an additional controller to the GSC, as well as the stable voltage control loop. Figure 5 shows the IEEE first benchmark modified by a DFIG-based wind farm with a WAMS and its controller. In addition, Figure 6 displays the location of the

fuzzy controller located in the GSC stator voltage control loop. In fact, using the WAMS and considering the time delays caused by sending measurement signals to the controller are some of the innovations of this paper. Therefore, this paper, as mentioned in [28], does not apply PLL for the WAMS, while PLL in [29] was used in the design of the controller.

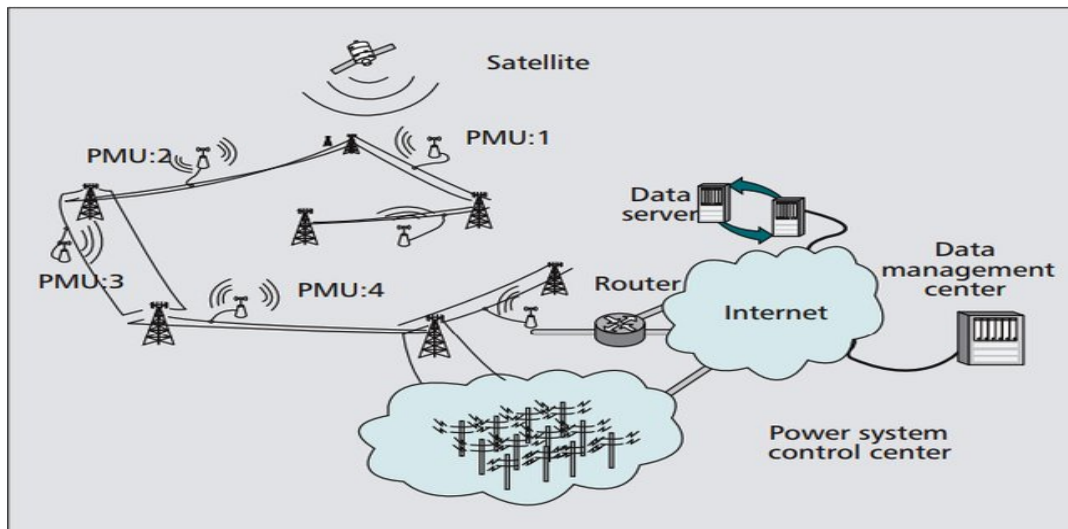


Figure 4. Hierarchical structure of a Wide Area Measurement System with PMUs.

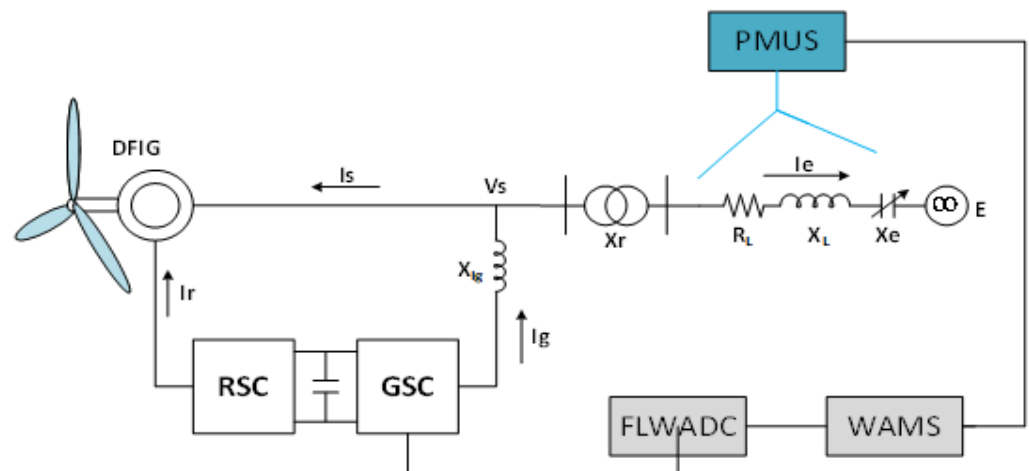


Figure 5. Location of fuzzy logic based on wide area in studied model.

Figure 6 shows the location of the fuzzy controller, which was applied to the input of the stator voltage control loop of the GSC.

4.1. Fuzzification

Fuzzy controller input is the capacitive compensating voltage (V_c) of the transmission line series and its changes ($\frac{dV_c}{dt}$), the membership function of which is considered as follows based on the fuzzy rules. Figure 7 displays the capacitor voltage with seven membership functions and its changes with three membership functions, as well as fuzzy controller output with seven membership functions, which is considered as the knowledge of an expert. As shown, the symbols were defined as negative large (NL), negative (NM), medium, negative small (NS), zero (ZE), positive small (PS), positive medium (PM), positive large (PL), negative (N), and positive (P).

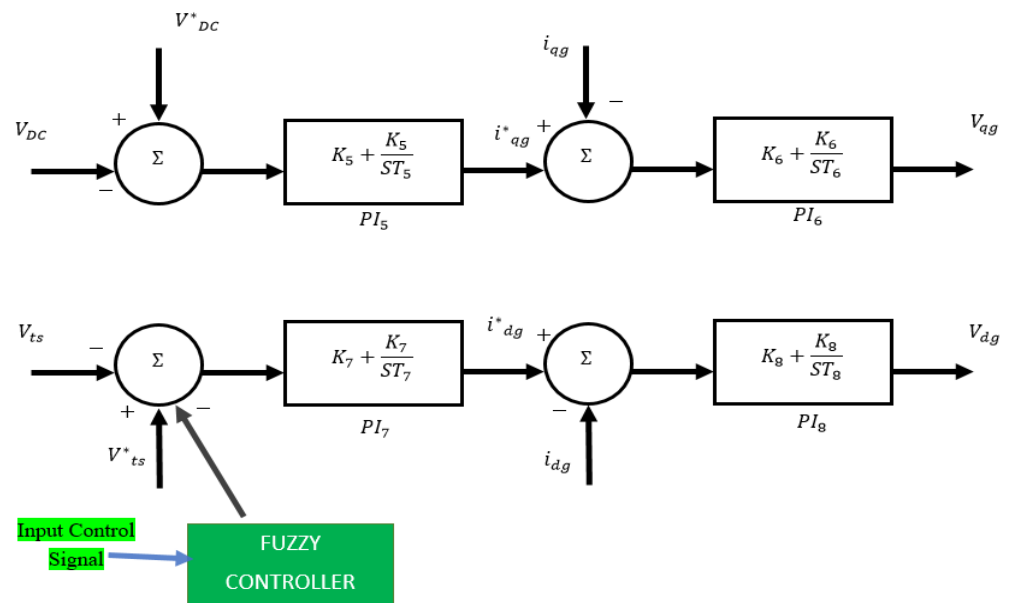


Figure 6. Location of Fuzzy logic System.

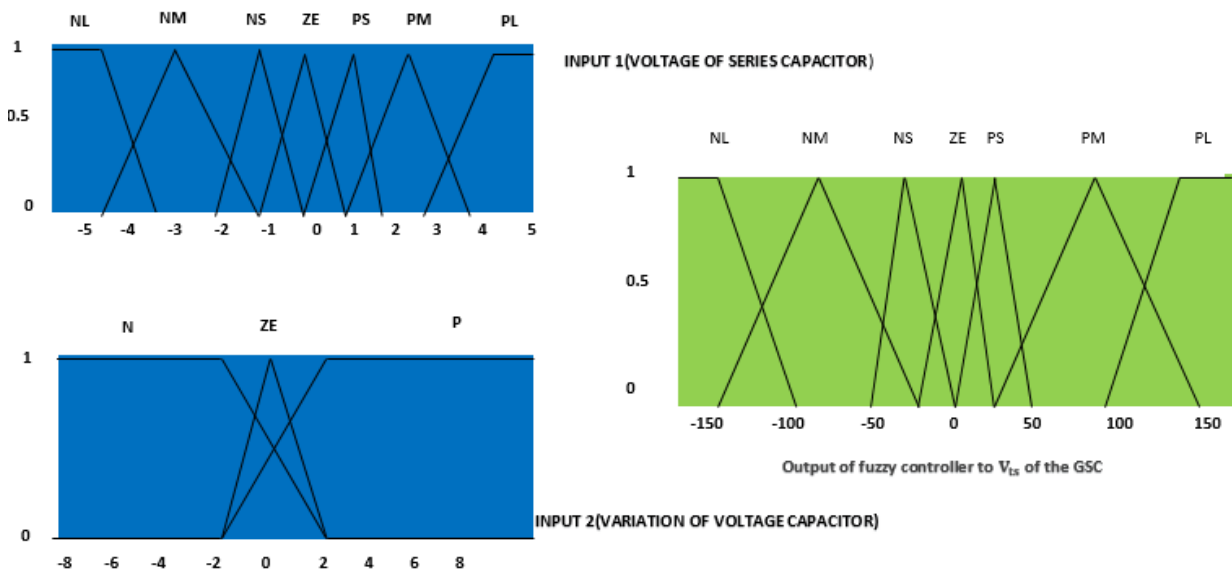


Figure 7. Inputs and output membership functions.

4.2. Rule Base and Inference Engine

As mentioned, the fuzzy rules were based on Mamdani type, in the form of “if then” and in the form of 21 fuzzy relations according to the inputs and outputs of the fuzzy system, as shown in Table 3. For instance, as shown in Table 3, if V_c was NS and $\frac{dV_c}{dt}$ was N, then the output was NM.

4.3. Defuzzification

Finally, the output of the fuzzy system was converted to a crisp number. In this study, the average center of gravity was used.

Table 3. Fuzzy rules based on fuzzy system inputs and output.

$V_c \backslash \frac{dV_c}{dT}$	P	N	ZE
PL	PL	PL	PL
PM	PL	PS	PM
PS	PM	ZE	PS
ZE	PM	NM	ZE
NS	ZE	NM	NS
NM	NS	NL	NM
NL	NM	NL	NL

5. Time-Domain Simulation Results

An IEEE-first-benchmark-modified, DFIG-based wind farm system was used to evaluate the proposed controller, and MATLAB/Simulink software was applied for simulating the time of the studied system. As mentioned before, the percentage of compensation of the transmission line is considered as one of the influential factors in SSR fluctuations, which increases with the percentage of compensation of the system towards instability. The modes of the studied system were expressed by using the eigenvalues method in Table 2, indicating that λ_1 and λ_2 were the oscillation modes of the system in the case where the compensation percentage was 25, 40, 60, and 75, as represented in Table 4. In this oscillating mode, the resonance frequency was 37.56 Hz, and the SSR frequency was 22.44 Hz. The contents of Equation (17) indicate an increase in the percentage of compensation, causing the resistance of the whole system to be negative, leading to instability in the system.

$$K\% \uparrow \Rightarrow X_c \uparrow \Rightarrow f_n = f_s \sqrt{\frac{X_c}{X}} \uparrow \Rightarrow s_n = \frac{f_n - f_r}{f_n} \downarrow \Rightarrow R_{eq-r} = \frac{R_r}{s_n} \uparrow \Rightarrow R_{eq} \leq 0 \quad (17)$$

Table 4. SSR mode and eigenvalues for compensation levels with wind speed 7 m/s.

Resonance Frequency	SSR Frequency	SSR Mode (λ_1 &2 Table 1)	Level of Compensation (%)
37.56	22.44	+11.650 + j130.21	75
35.74	24.26	+5.760 + j148.35	60
30.46	29.54	−1.25 + j185.54	40
22.8	37.2	−4.66 + j231.20	25

Figure 8 shows the compensation system in the case where the compensation percentage was 25 and the system was stable. In the third second of the simulation, the compensation percentage increased to 75, and the parameters were unstable.

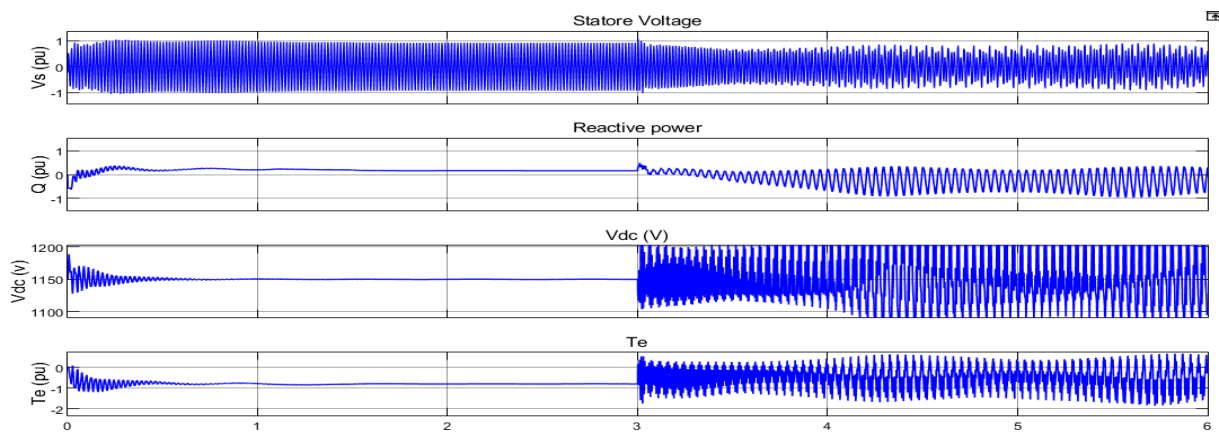


Figure 8. Capacitor voltage, reactive power stator voltage, and electrical torque in $k = 25\%$ to $k = 75\%$ & $v = 7$ m/s without damping.

5.1. FLWADC without Time Delay

This part of the simulation showed the application of the fuzzy controller to the studied system in the case where the delays caused by the measured PMU signals were ignored. As shown in Figure 8, SSR fluctuations were damped by applying a controller to the stator voltage control loop in the GSC. As mentioned, the residue-based analysis method was used to select the input control signal, rotor speed (ω_r), and voltage across the series compensation (V_c).

The transfer function $G(s)$ can be factored as given in (18):

$$G(s) = \frac{R_i}{s - \lambda_i} \quad (18)$$

where λ_i is the eigenvalues, and R_i is the residues of the eigenvalues [30]. By obtaining the value of R_i for the sub-synchronous mode corresponding to λ_1 and λ_2 of Table 1, the location of the controller and the capacitor voltage could be selected as the input control signal.

The membership functions of Figure 7 were quenched by the SSR fluctuations with the 21 fuzzy rules in Table 3 and receiving the controller inputs, which were the same as the capacitor compensating voltage and its changes from the PMU, as shown in Figure 5.

As displayed in Figure 9, the oscillations were damped in the case where the compensation percentage was 75, and the system was made unstable in the third second of the simulation by applying a fuzzy controller (FLWA).

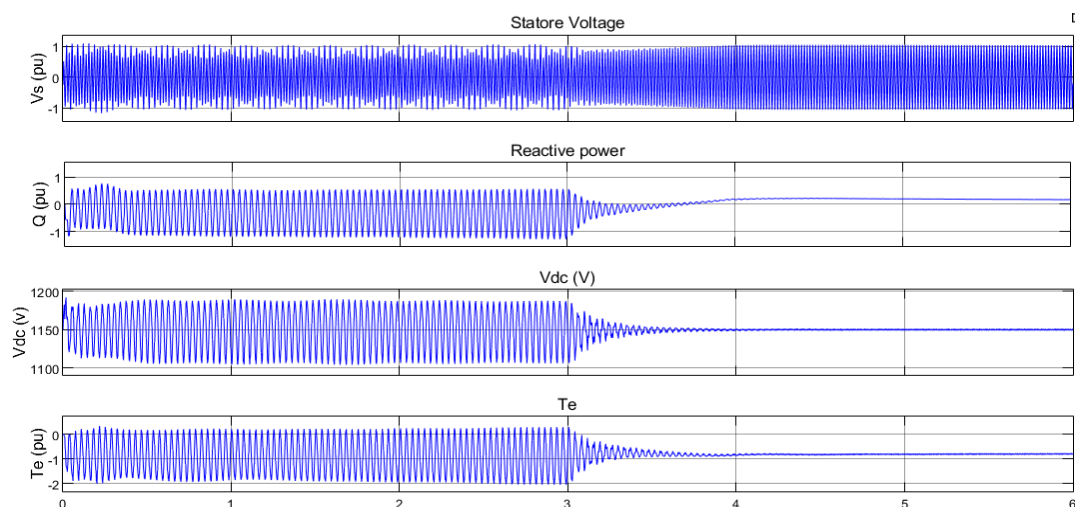


Figure 9. Damping of capacitor voltage, reactive power stator voltage, and electrical torque in $k = 75\%$ & $v = 7$ m/s with FLWADC (ignoring time delay).

5.2. Robust FLWADC with Latency Compensation

In the previous section, WAMS-based fuzzy controller simulations were performed in which the latencies due to PMU measurement signals were ignored. In fact, these time delays in sending signals to the controller cannot be ignored since delays are inevitable in telecommunication systems, as shown in Table 5. Table 5 shows the communication links and associated delay in a WAMS [31].

Table 5. Time delay in various communication links [31].

Communication Link	Associated Delay (ms)
Fiber-optic cables	100–150
Digital microwave link	100–150
PLC	150–350
Telephone lines	200–350
Satellite link	500–700

To consider the delays caused by measuring PMU signals, the third input was modeled for another fuzzy input to the fuzzy controller (Figure 10). As shown, delays were considered in small (S), medium (M), and large (L) membership models. For simplicity, low delays (S) were equivalent to no delays.

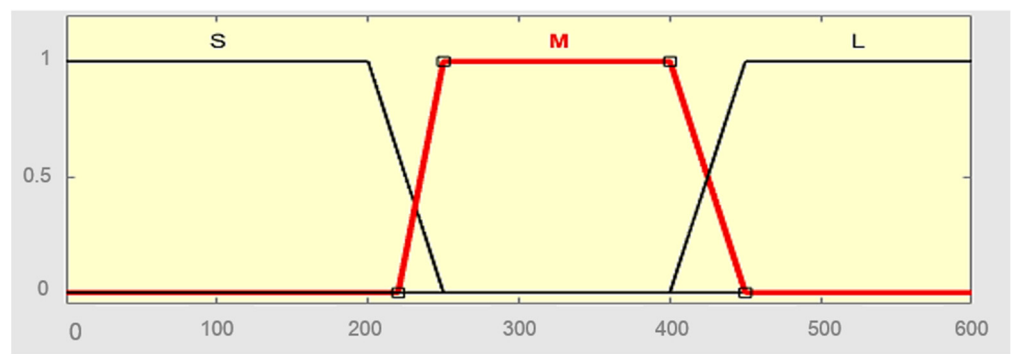


Figure 10. Membership functions of the latency variable for robust FLWADC.

The fuzzy rules of Table 3 changed for applying this fuzzy input to the fuzzy system, the cause of which is shown in Figure 11. In addition, the series-compensating capacitor voltage was demonstrated in without-delay (a), medium-delay (b), and long-delay (c) modes.

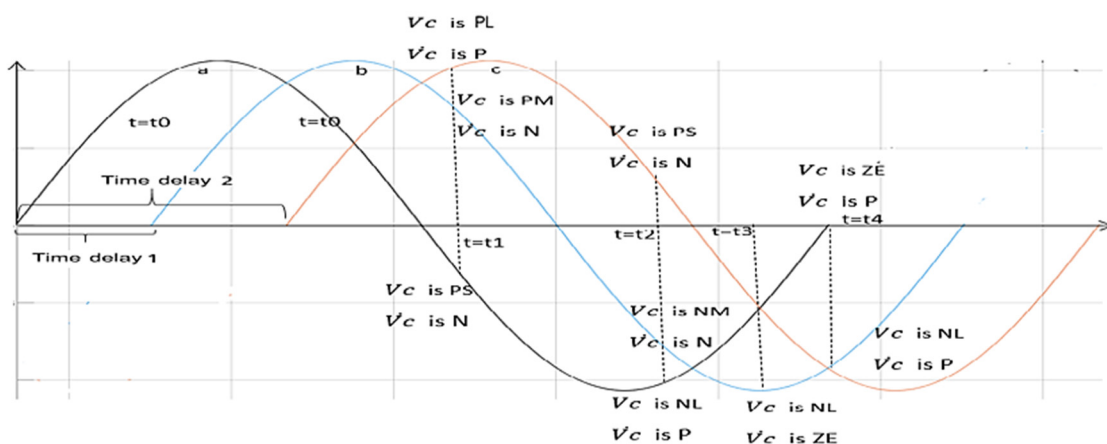


Figure 11. Time-delay signal of V_c .

Consider the moment $t = t_1$ as an example. At this point, the main signal was the no-delay input where V_c was PS and $\frac{dV_c}{dt}$ was N, which means that the output value of the fuzzy controller equaled ZE. However, if the medium delay was M: time delay 1, the fuzzy rule in this delay, V_c was PM and

$\frac{dV_c}{dt}$ was N, was the output of system the ZE. Further, if the delays were large, L is time delay 2, and the fuzzy rule in this delay was V_c was PL and $\frac{dV_c}{dt}$ was P, the output of the fuzzy system in this delay was ZE. Similarly, other modified fuzzy rules were shown by considering the delays in Table 6.

Table 6. Rule based on delay-compensated FLWADC.

Time Delay	$V_c \backslash \frac{dV_c}{dt}$	PL	PM	PS	ZE	NS	NM	NL
M	P	PS	NL	PL	PM	PM	NM	PM
	N	NL	ZE	PM	NL	NS	NM	PS
	ZE	NS	PS	NM	ZE	PL	NM	NL
L	P	ZE	PM	PL	NM	NL	NM	PM
	N	PL	ZE	NM	PM	PM	PS	NM
	ZE	PS	NL	ZE	PL	NM	ZE	PL

By changing the fuzzy rules, which were modeled by considering the delays caused by PMU measurement signals, the simulation of the studied system with two time delays of 350 and 500 ms was performed, as shown in Figures 12 and 13. As shown, the fuzzy controller damped the fluctuations caused by SSR by considering the changes in fuzzy rules. In this simulation, the compensation percentage was 75 and wind speed was 7 m/s.

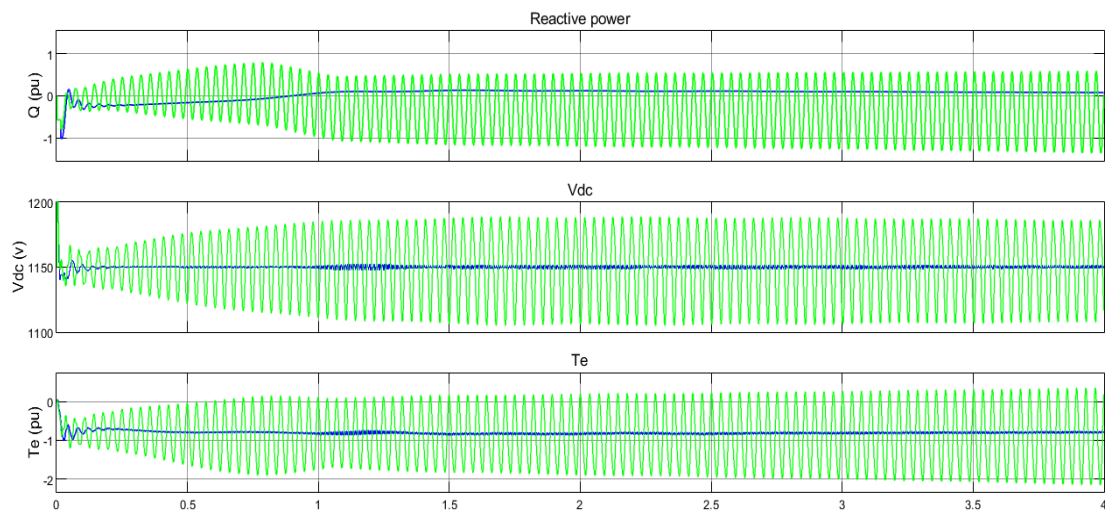


Figure 12. Damping of capacitor voltage, reactive power, and electrical torque in $k = 75\%$, $v = 7$ m/s with new FLWADC and time delay equal to 350 ms in comparison without control.

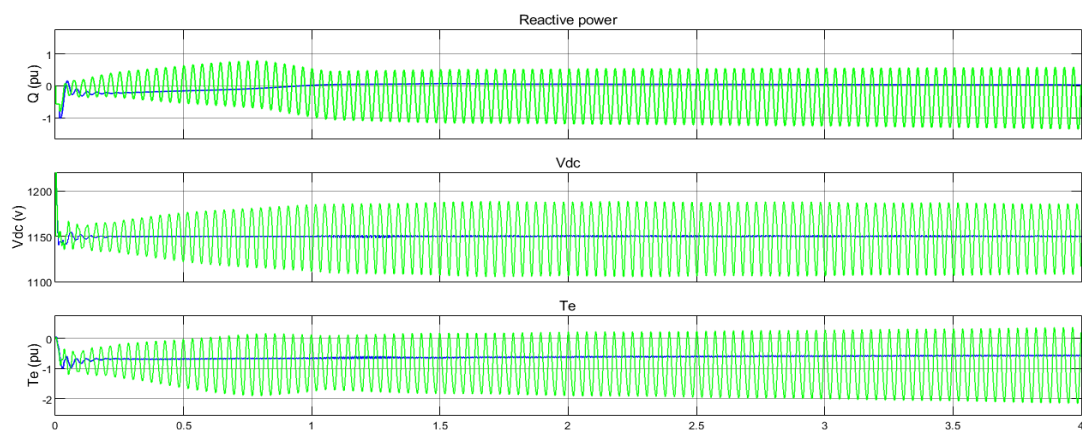


Figure 13. Damping of capacitor voltage, reactive power, and electrical torque in $k = 75\%$, $v = 7$ m/s and time delay 500 ms with the proposed FLWADC and without control.

Figure 14 shows that the state that the measurement signals applied to the fuzzy controller had a delay of 350 ms, and the actions of the controller in the first second caused system instability and failed to dampen the system if latency is ignored.

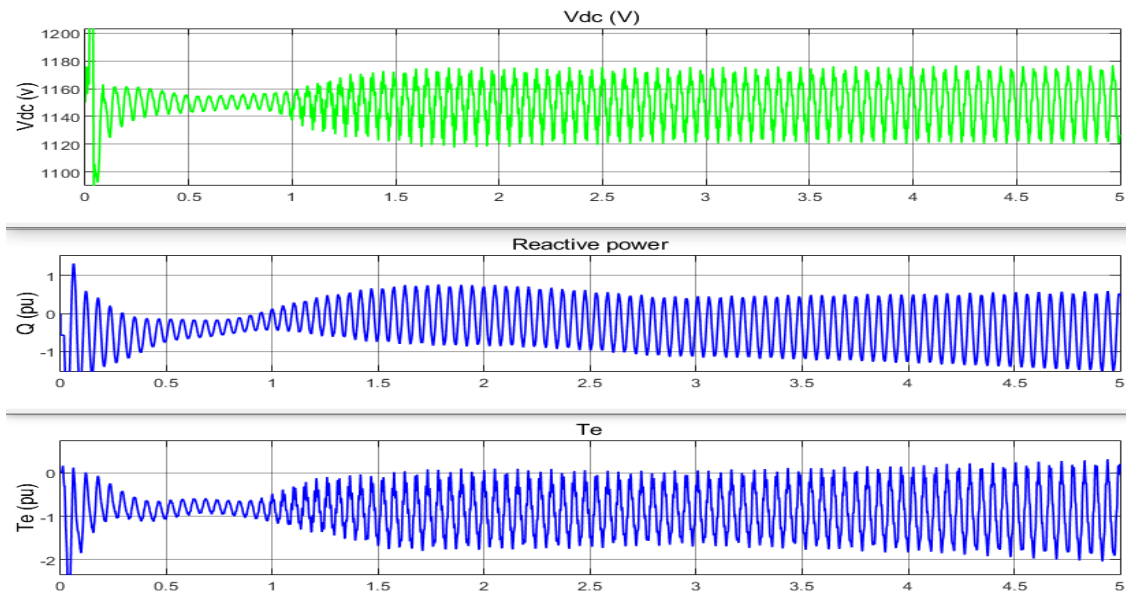


Figure 14. Capacitor voltage, reactive power, and electrical torque in $k = 75\%$ and $v = 7$ m/s with FLWADC. Ignored latency in time delay equal 500 ms.

6. Conclusions

This paper proposed a novel approach for mitigating sub-synchronous resonance (SSR) in DFIG-based wind farms installed in a microgrid with a wide-area monitoring system (WAMS). The proposed approach does not require adjusting the parameters of the controller. Additionally, it enables a high level of compensation, namely 75%, and takes into consideration time delays caused by PMU measurements in the control design phase. Delay is important because it can cause system instability if ignored. The proposed FLWADC was implemented to a modified IEEE first benchmark model with a DFIG. Its performance in damping SSR fluctuations was demonstrated using time simulations carried out using MATLAB/Simulink software. The obtained results confirmed the controller's ability to effectively damp SSR and ensure system stability whilst taking into consideration PMU delays.

Author Contributions: Conceptualization, investigation, and writing—original draft preparation, Y.B., S.J. and S.M.; writing—review and editing and supervision, A.F. and W.A. All authors have read and agreed to the published version of the manuscript.

Funding: The authors received no financial support for the research, authorship, and/or publication of this article.

Institutional Review Board Statement: Not applicable.

Informed Consent Statement: Not applicable.

Data Availability Statement: Not applicable.

Conflicts of Interest: The authors declare that they have no conflict of interest.

Nomenclature

SSR	Sub-synchronous resonance
Wams	Wide-area measurement system
Pmu	Phasor measurement unit
IGE	Inductive generating effects
DFIG	Doubly fed induction generator
TI	Torsional interference
IGE	Induction generator effect
GSC	Grid-side convertor
RSC	Rotor-side convertor
ω_r	Rotor frequency
ω_b	Synchronous frequency

Appendix A

Table A1. Parameters of the single line diagram of the DFIG-based WT.

Base power	2 MW	100 MW
Based voltage (VLL)	690 V	690 V
Xls	0.09231	0.09231
Xlr	0.09955	0.09955
Rs	0.00488	0.00488
XM	3.95279	3.95279
Xtg	0.3 (0.189 mH)	0.3 (0.189/50 mH)
DC-link base voltage	1200 V	1200 V
DC-link capacitor	14,000 μ F	50 \times 14,000 μ F

References

1. CIGRE Working Group C4/B5.41. *Challenges with Series Compensation Applications in Power Systems When Overcompensating Lines*; Technical Report; CIGRE: Paris, France, 2021.
2. Xiong, H.; Egusquiza, M.; Østergaard, P.A.; Pérez-Díaz, J.I.; Sun, G.; Egusquiza, E.; Luo, X. Multi-objective optimization of a hydro-wind-photovoltaic power complementary plant with a vibration avoidance strategy. *Appl. Energy* **2021**, *301*, 117459. [\[CrossRef\]](#)
3. Xiong, H.; Xu, B.; Kheav, K.; Luo, X.; Zhang, X.; Patelli, E.; Chen, D. Multiscale power fluctuation evaluation of a hydro-wind-photovoltaic system. *Renew. Energy* **2021**, *175*, 153–166. [\[CrossRef\]](#)
4. Raju, D.K.; Umre, B.S.; Junghare, A.S.; Babu, B.C. Mitigation of subsynchronous resonance with fractional-order PI based UPFC controller. *Mech. Syst. Signal Process.* **2017**, *85*, 698–715. [\[CrossRef\]](#)
5. Xu, L.; Cartwright, P. Direct active and reactive power control of DFIG for wind energy generation. *IEEE Trans. Energy Convers.* **2006**, *21*, 750–758. [\[CrossRef\]](#)
6. Jiao, Y.; Li, F.; Dai, H.; Nian, H. Analysis and mitigation of sub-synchronous resonance for doubly fed induction generator under VSG control. *Energies* **2020**, *13*, 1582. [\[CrossRef\]](#)
7. Piwko, R.; Miller, N.; Sanchez-Gasca, J.; Yuan, X.; Dai, R.; Lyons, J. Integrating large wind farms into weak power grids with long transmission lines. In Proceedings of the 5th International Power Electronics and Motion Control Conference, Shanghai, China, 14–16 August 2006; Volume 2, pp. 1–7.
8. Mohammadpour, H.A.; Santi, E. Optimal adaptive sub-synchronous resonance damping controller for a series-compensated doubly-fed induction generator-based wind farm. *IET Renew. Power Gener.* **2015**, *9*, 669–681. [\[CrossRef\]](#)
9. Fan, L.; Zhu, C.; Miao, Z.; Hu, M. Modal analysis of a DFIG-based wind farm interfaced with a series compensated network. *IEEE Trans. Energy Convers.* **2011**, *26*, 1010–1020. [\[CrossRef\]](#)
10. Sahni, M.; Badrzadeh, B.; Muthumuni, D.; Cheng, Y.; Yin, H.; Huang, S.-H.; Zhou, Y. Sub-synchronous interaction in Wind Power Plants-part II: An ERCOT case study. In Proceedings of the 2012 IEEE Power and Energy Society General Meeting, San Diego, CA, USA, 22–26 July 2012; pp. 1–9.
11. Fan, L.; Kavasseri, R.; Miao, Z.L.; Zhu, C. Modeling of DFIG-based wind farms for SSR analysis. *IEEE Trans. Power Deliv.* **2010**, *25*, 2073–2082. [\[CrossRef\]](#)
12. Wang, L.; Xie, X.; Jiang, Q.; Pota, H.R. Mitigation of multimodal subsynchronous resonance via controlled injection of supersynchronous and subsynchronous currents. *IEEE Trans. Power Syst.* **2013**, *29*, 1335–1344. [\[CrossRef\]](#)
13. Xie, H.; de Oliveira, M.M. Mitigation of SSR in presence of wind power and series compensation by SVC. In Proceedings of the IEEE 2014 International Conference on Power System Technology, Chengdu, China, 20–22 October 2014; pp. 2819–2826.

14. El-Moursi, M.S.; Bak-Jensen, B.; Abdel-Rahman, M.H. Novel STATCOM controller for mitigating SSR and damping power system oscillations in a series compensated wind park. *IEEE Trans. Power Electron.* **2009**, *25*, 429–441. [[CrossRef](#)]
15. Tapia, A.; Tapia, G.; Ostolaza, J.X.; Saenz, J.R. Modeling and control of a wind turbine driven doubly fed induction generator. *IEEE Trans. Energy Convers.* **2003**, *18*, 194–204. [[CrossRef](#)]
16. Xu, L.; Wang, Y. Dynamic modeling and control of DFIG-based wind turbines under unbalanced network conditions. *IEEE Trans. Power Syst.* **2007**, *22*, 314–323. [[CrossRef](#)]
17. Hughes, F.M.; Anaya-Lara, O.; Jenkins, N.; Strbac, G. A power system stabilizer for DFIG-based wind generation. *IEEE Trans. Power Syst.* **2006**, *21*, 763–772. [[CrossRef](#)]
18. Bialasiewicz, J.T.; Muljadi, E. The wind farm aggregation impact on power quality. In Proceedings of the 32nd Annual Conference on IEEE Industrial Electronics IECON 2006, Paris, France, 7–10 November 2006; pp. 4195–4200.
19. Vajpayee, S.; Panda, N.R.; Behera, P.; Swain, S.C. Implementation of PLL algorithm in DFIG based wind turbine connected to utility grid. In Proceedings of the IEEE 2020 Second International Conference on Inventive Research in Computing Applications (ICIRCA), Coimbatore, India, 15–17 July 2020; pp. 549–553.
20. Liu, H.; Xie, X.; Li, Y.; Liu, H.; Hu, Y. Mitigation of SSR by embedding subsynchronous notch filters into DFIG converter controllers. *IET Gener. Transm. Distrib.* **2017**, *11*, 2888–2896. [[CrossRef](#)]
21. Musarrat, M.N.; Fekih, A.; Islam, M.R. An Improved Fault Ride Through Scheme and Control Strategy for DFIG-Based Wind Energy Systems. *IEEE Trans. Appl. Supercond.* **2021**, *31*, 1–6. [[CrossRef](#)]
22. Momoh, J.A.; Ma, X.W.; Tomsovic, K. Overview and literature survey of fuzzy set theory in power systems. *IEEE Trans. Power Syst.* **1995**, *10*, 1676–1690. [[CrossRef](#)]
23. Suriyaarachchi, D.H.R.; Annakkage, U.D.; Karawita, C.; Kell, D.; Mendis, R.; Chopra, R. Application of an SVC to damp sub-synchronous interaction between wind farms and series compensated transmission lines. In Proceedings of the 2012 IEEE Power and Energy Society General Meeting, San Diego, CA, USA, 22–26 July 2012; pp. 1–6.
24. Mohammadpour, H.A.; Ghaderi, A.; Mohammadpour, H.; Santi, E. SSR damping in wind farms using observed-state feedback control of DFIG converters. *Electr. Power Syst. Res.* **2015**, *123*, 57–66. [[CrossRef](#)]
25. Xie, H.; Li, B.; Heyman, C.; De Oliveira, M.M.; Monge, M. Subsynchronous resonance characteristics in presence of doubly-fed induction generator and series compensation and mitigation of subsynchronous resonance by proper control of series capacitor. *IET Renew. Power Gener.* **2014**, *8*, 411–421. [[CrossRef](#)]
26. Chaudhuri, N.R.; Ray, S.; Majumder, R.; Chaudhuri, B. A new approach to continuous latency compensation with adaptive phasor power oscillation damping controller (POD). *IEEE Trans. Power Syst.* **2009**, *25*, 939–946. [[CrossRef](#)]
27. Tomsovic, K.; Tapper, M.; Ingvarsson, T. A fuzzy information approach to integrating different transformer diagnostic methods. *IEEE Trans. Power Deliv.* **1993**, *8*, 638–1646. [[CrossRef](#)]
28. Naduvathuparambil, B.; Valenti, M.C.; Feliachi, A. Communication delays in wide-area measurement systems; Cat. No. 02EX540. In Proceedings of the IEEE Thirty-Fourth Southeastern Symposium on System Theory, Huntsville, AL, USA, 19 March 2002; pp. 118–122.
29. Fateh, D.; Birjandi, A.A.M.; Guerrero, J.M. A subsynchronous resonance prevention for DFIG-based wind farms. *Turk. J. Electr. Eng. Comput. Sci.* **2020**, *28*, 2670–2685. [[CrossRef](#)]
30. Miller, N.W.; Sanchez-Gasca, J.J.; Price, W.W.; Delmerico, R.W. Dynamic modeling of GE 1.5 and 3.6 MW wind turbine-generators for stability simulations; Cat. No. 03CH37491. In Proceedings of the 2003 IEEE Power Engineering Society General Meeting, Toronto, ON, Canada, 13–17 July 2003; Volume 3, pp. 1977–1983.
31. Mohammadpour, H.A.; Shin, Y.J.; Santi, E. SSR analysis of a DFIG-based wind farm interfaced with a gate-controlled series capacitor. In Proceedings of the Applied Power Electronics Conference and Exposition-APEC 2014, Fort Worth, TX, USA, 16–20 March 2014; pp. 3110–3117.